3. Copper-organic complexes synthetized electrochemically

The anode coupons at the end of the experiments with carboxylate acids, lactose and casein contained deposit varying in shades of blue/green (Fig 3.1).

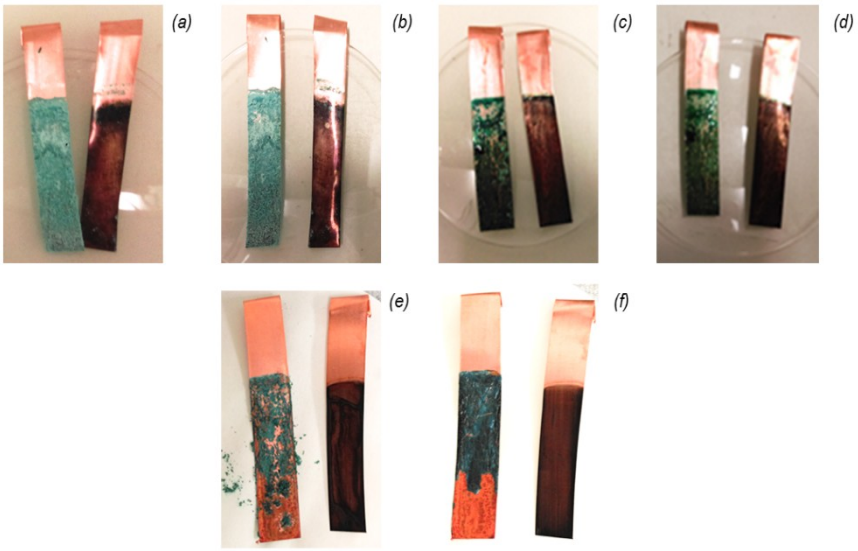

Fig 3.1 – Copper coupons at the end of experiments anode coupons are those on the left, following exposure to palmitic acid (a), stearic acid (b), oleic acid (c), linoleic acid (d), lactose (e) and casein (f)

3.1. Characterization of Copper Soaps

The (+) coupons from the electrolyte containing palmitic and stearic acids were covered by a light greenish/blue powdery deposit (Fig 3.1a-b) whilst those exposed to oleic and linoleic acids were covered by a dark green, reflective sticky film (Fig 3.1c-d). For ease of reference, these deposits will be referred to as Cu-Palmitate, Cu-Stearate, Cu-Oleate and Cu-Linoleate respectively.

3.1.1 Analysis by Fourier Transform Infrared Spectrocopy (FTIR)

Carboxylic acids normally exist as dimers due to strong intermolecular hydrogen bonding [1] characterized by hydroxyl (OH) and carbonyl (C=O) vibrations. Their most recognizable OH vibrations are a broad band in the 3300-2500cm^{-1} region and a variable intensity band around 955-890cm^{-1}, whilst the C=O vibration appears as a strong band within 1715-1680cm^{-1} region. When ionization occurs forming the COO^- carboxylate ion, resonance is possible between the two C-O bonds [2]. The C=O band is replaced by two vibrations: a characteristic strong band between 1610-1550cm^{-1} (COO^- asymmetric stretching) and a medium band between 1420-1300cm^{-1}(COO^- symmetric stretching) [3].

The COO^- bands in Cu-Palmitate appear as a strong band around 1583cm^{-1} and a medium band around 1422cm^{-1}. The appearance of these bands coincide with the reduction of the C=O band around 1700cm^{-1} (Fig 3.2b).

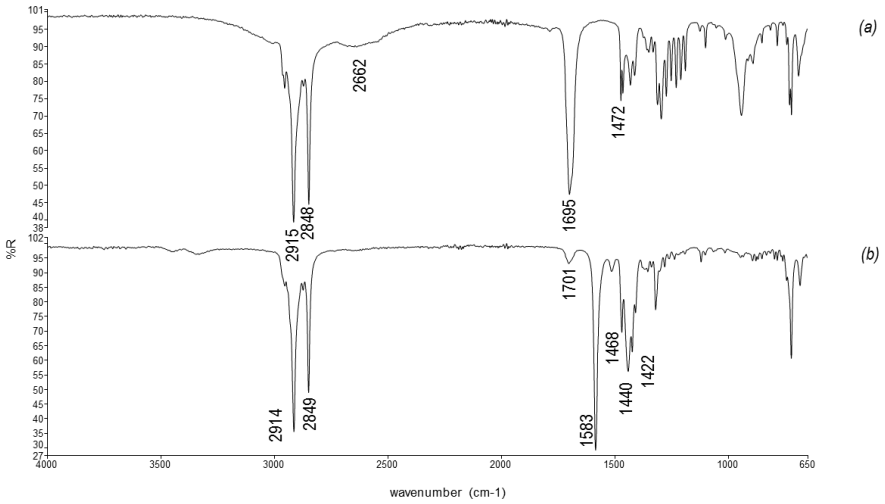

Fig 3.2 - FTIR spectra of Palmitic Acid (a) and Cu-Palmitate (b) obtained in ATR mode

Analogous bands to Cu-Palmitate were also identified in the spectra of the remaining copper soaps (Table 3.1).

Cu-Palmitate	Cu-Stearate	Cu-Oleate	Cu-Linoleate	Band Assignment
2914 vs	2912 vs	2916 vs	2924 vs	C-H stretching vibrations
2849 vs	2846 vs	2849 s	2853 s	C-H stretching vibrations
1701 m	1695 w,br		1729 m	C=O (dimer) stretching
1583 vs	1585 vs	1583 vs	1601 vs	COO^- asymmetric stretching vibrations
1422 m	1419 m	1414 m	1413 m	COO^- symmetric stretching vibrations
946 vw				OH deformation
721 m	716 m	718 w		COO^- scissor vibrations
682 m	673 m			COO^- wagging vibrations

vs (very strong), s (strong), m (medium), w (weak)

Table 3.1. Characteristic FTIR bands of Copper Soaps

The peaks at around 1700cm^{-1} and at 950cm^{-1} are due to the presence of acid residues - unreacted acid or resulting from the behavior of the carboxylate ions in aqueous medium [4] according to the following reactions:

$$2H_2O \rightleftharpoons H_3O^+ + OH^-$$
$$RCOO^- + H_3O^+ \rightleftharpoons RCOOH + H_2O$$

The (+) coupons containing the copper soaps were also analysed by FTIR with an ATR microscope attachment (Fig 3.3). The main advantage of using an ATR microscope is that it enables spatially resolved analysis without sample removal, ideal for the study of paintings and manuscripts. The obtained spectra for Cu-Palmitate and Cu-Stearate contain a well-defined peak corresponding to asymmetric COO^- stretching vibrations (area within a rectangle in Figure 3.3), practically non-existent in Cu-oleate and Cu-linoleate spectra. This may explain why unsaturated copper soaps are not reported in FTIR-ATR analyses in the literature [5-7].

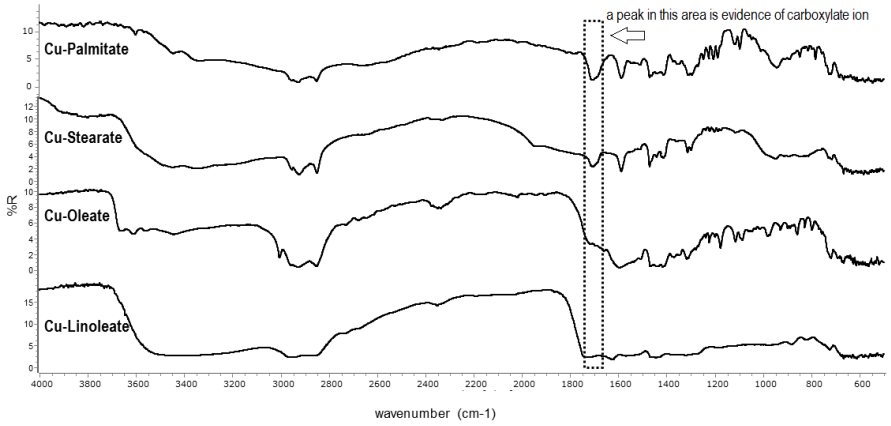

Fig 3.3 – FTIR spectra of Copper Soaps obtained with ATR microscope

3.1.2 Analysis by Raman Spectroscopy

Theoretical and experimental studies have assigned bands below 590cm^{-1} in the infrared and Raman spectra of metal-organic complexes to metal-nitrogen (M-N) and metal-oxygen (M-O) vibrations [1, 3]. Cu-O vibrations have been specifically assigned to bands in the 350-180cm^{-1} region for copper(II) acetate [8-9], copper(II) hexanoate [10] copper palmitate and copper stearate [11]. The bands at 307cm^{-1} and 255cm^{-1} in Cu-Palmitate's spectrum (Fig 3.4b), which do not appear in the spectrum of palmitic acid (Fig 3.4a), may be attributed to Cu-O vibrations and thus considered evidence of metal-organic complexation. Similar bands were also identified in the spectra of Cu-Stearate and Cu-Oleate but not in Cu-Linoleate due to fluorescence (Figure 3.5d).

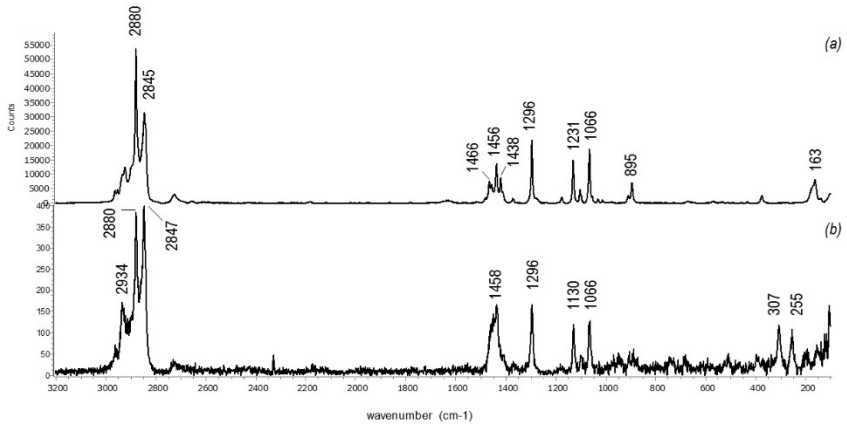

Fig 3.4 - Raman spectra of Palmitic Acid (a) and Cu-Palmitate (b) baseline corrected

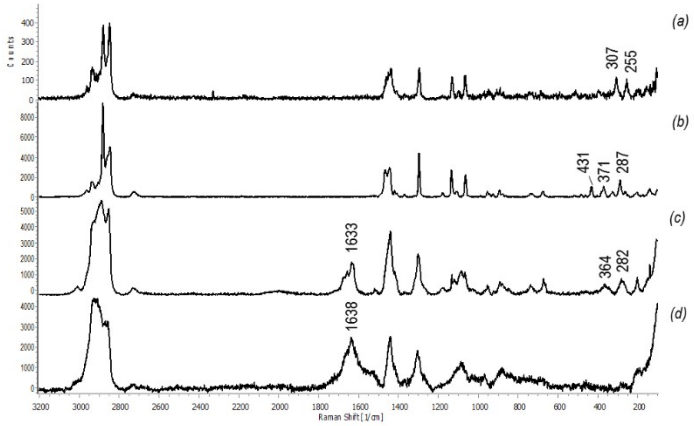

Fig 3.5 - Raman spectra of Cu-Palmitate (a), Cu-Stearate (b), Cu-Oleate (c) and Cu-Linoleate (d)

The main difference between the copper soaps' spectra is the broad peak at around 1630cm^{-1} in Cu-Oleate and Cu- Linoleate (Figure 3.5c-d and Table 3.2). This peak corresponds to the C=C bond(s), which are very weak in FTIR.

Cu-Palmitate	Cu-Stearate	Cu-Oleate	Cu-Linoleate	Band Assignments
2934 m	2931 m	3007 m	2920 s	C-H stretching vibrations
2880 m	2880 vs	2867 s	2867 s	C-H stretching vibrations

2847 vs	2847 vs			C-H stretching vibrations
		1633 s	1638 s	C=C stretching vibrations
1556 vw	1523 vw	1517 w		COO^- asymmetric stretching vibration
1437 s	1442 s	1440 s	1440 s	CH_2 scissors aliphatic
1296 s	1297 s	1301 s	1302 s	CH_2 torsion
1130 s	1132 s	1132 s		C-C vibrations
1066 s	1063 s	1070 s	1085 s	COO^- deformation
	431 m			Cu-O vibration
	371 m	364 m		Cu-O vibration
307 m				Cu-O vibration
	287 m	282 m		Cu-O vibration
255 m				Cu-O vibration

vs (very strong), s (strong), m (medium), w (weak), vw (very weak)

Table 3.2 - Characteristic Raman bands of copper soaps

3.1.3 Analysis by X-ray Photoelectron Spectroscopy (XPS)

The elemental composition obtained by XPS shows an agreement between theoretical and experimental values for Cu-Palmitate and Cu-Oleate, but deviations for Cu-Stearate of 11% and of 61% for Cu-Linoleate (Table 3.3). The high deviation obtained for Cu-Linoleate is likely to result from the decomposition of the sample prior to or during analysis but invisible to the naked eye.

		Relative Atomic %			C:O:Cu	
	Ligand Formula	C1s	O1s	Cu2p	Theoretical	Experimental*
Palmitic Acid	$C_{16}H_{32}O_2$	89.32	10.62	-	32:4:0	34:4:0
Cu-Palmitate	$C_{16}H_{32}O_2$	85.53	10.72	2.81	32:4:1	32:4:1
Cu-Stearate	$C_{18}H_{36}O_2$	84.62	10.62	2.93	36:4:1	32:4:1
Cu-Oleate	$C_{18}H_{34}O_2$	87.97	9.81	2.25	36:4:1	36:4:1
Cu-Linoleate	$C_{18}H_{32}O_2$	68.93	24.23	3.00	36:4:1	11:4:1

*rounded to the closest integer

Table 3.3 - Elemental Composition and Atomic Proportions for palmitic acid and copper soaps

Cu(II) ions can be differentiated from Cu(I) ions, independent of the ligand, by the presence of shake-up (or satellite) peaks in their Cu2p spectrum in the regions below 960eV and between 945-940eV [12-14]. The Cu2p spectra for all copper soaps analysed contain satellite peaks in these regions confirming the presence of Cu(II) ions.

Evidence of metal complexation can be obtained by comparing the high-resolution spectra of C1s and O1s regions of the carboxylic acid and its copper soap.

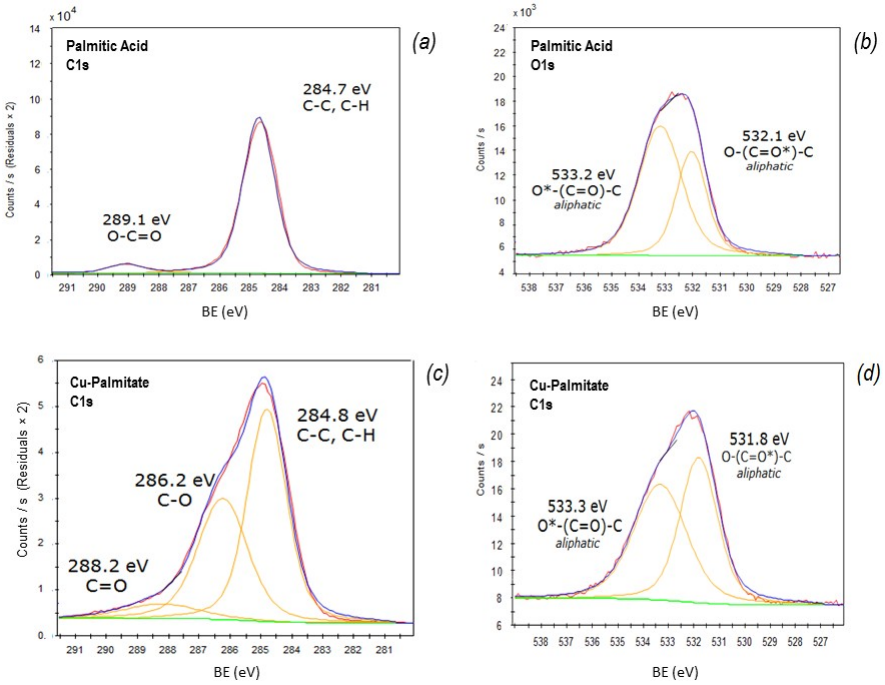

Fig 3.6. Spectra of C1s and O1s regions of Palmitic Acid (a-b) and Cu-Palmitate (c-d)

Palmitic acid's C1s spectrum contains two well defined peaks (Fig 3.6a). One peak is centered at 284.7eV corresponding to C-C/C-H bonds in a carbon chain and another at 289.1eV corresponding to a carbon coordinated to oxygen atoms, O-C=O. In contrast, the C1s spectrum for Cu-Palmitate (Fig 3.6b) shows a single large peak. This peak can be decomposed into a peak at 284.8eV corresponding to C-C/C-H and two further two peaks for the carboxylate carbon. One peak at 286.2eV can be assigned to C-C=O [15] and another peak at 288.2eV to C-O [16].

The O1s spectra of palmitic acid (Fig 3.6c) also differs from that obtained for Cu-Palmitate (Fig 3.6d). The binding energy (BE) of the O=C decreases from 532.1 to 531.8eV with an increase in the O-C from 533.2 to 533.3eV. Similar values were also observed for the remaining copper soaps (Table 3.4).

Region	Chemical Bonds	Cu-Palmitate	Cu-Stearate	Cu-Oleate	Cu-Linoleate
C1s BE (eV)	C-C, C-H, C=C	284.8	284.6	284.6	284.4
	C-O	286.2	285.8	285.9	285.9
	C=O, C-O-Cu	288.2	287.8	288.7	288.2

O1s	O-(C=O*)-C	531.8	531.7	531.7	531.6
BE (eV)	O*-(C=O)-C	533.3	533.1	533.0	532.8

Table 3.4 - C1s and O1s peaks binding energies (BE) for copper soaps

As the position of an XPS peak for an atom is affected by the initial binding energy of the electron in its orbital, any changes in the atom's vicinity are likely to shift peak positions. However, copper soaps exist as coordination complexes where the bond between the metal ion and the organic component is often delocalized, without having a distinct covalent or ionic character. Hence, the chemical shifts imposed by the metal ion on the carboxylic function cannot be easily measured by this technique.

3.1.4 Analysis by X-ray Diffraction (XRD)

Diffraction patterns were obtained between 5-40º 2θ for Cu-Palmitate (Table 3.5), Cu-Stearate (Table 3.6) and Cu-Oleate (Table 3.7). No diffraction pattern was obtained for Cu-Linoleate.

Below 25º 2θ, the intensity and position of the peaks appear to correlate with the length of the carbon chain and its level of unsaturation. An increase in the carbon chain (from C16 in Cu-Palmitate to C18 in Cu-Stearate) resulted in a shift in peak positions to lower angles, analogous to the acid forms as reported in the literature [11].

2θ (º)	d-spacings (nm)	I/Iº (%)	2θ (º)	d-spacings (nm)	I/Iº (%)
5.991	**1.4739**	**28.3**	18.522	0.4787	1.3
6.246	**1.4139**	**100.0**	18.989	0.4670	1.5
7.435	**1.1880**	**34.7**	19.385	0.4575	3.5
8.353	1.0576	10.8	19.893	0.4460	3.4
8.812	1.0027	0.8	20.443	0.4341	1.9
9.196	0.9607	1.7	20.813	0.4265	2.1
9.901	0.8927	10.4	**21.612**	**0.4109**	**43.1**
10.462	0.8449	18.6	22.463	0.3955	1.5

11.129	0.7944	4.2	22.866	0.3886	3.7
11.739	0.7533	5.2	23.135	0.3842	10.8
11.878	0.7445	5.7	23.803	0.3735	4.4
12.402	0.7131	12.0	24.207	0.3674	22.4
13.315	0.6644	1.9	27.212	0.3276	1.0
13.755	0.6433	1.9	27.625	0.3227	0.6
14.548	0.6084	2.5	29.083	0.3068	1.0
15.799	0.6047	1.1	30.26	0.2951	3.0
17.367	0.5102	1.1			

Table 3.5 – X-ray powder diffraction pattern obtained for Cu-Palmitate, most intense peaks in BOLD

2θ (°)	d-spacings (nm)	I/I° (%)	2θ (°)	d-spacings (nm)	I/I° (%)
5.272	**1.6749**	**39.8**	13.145	0.6730	6.5
5.611	**1.5739**	**100.0**	14.071	0.6289	0.6
7.012	1.2596	9.0	15.047	0.5883	0.5
7.499	1.1779	14.5	15.846	0.5588	0.7
8.772	1.0073	10.2	16.188	0.5471	0.6
8.959	0.9862	3.9	16.94	0.5230	1.1
9.375	**0.9426**	**26.9**	19.385	0.4575	1.0
10.528	0.8396	2.2	19.752	0.4491	0.5
10.851	0.8147	0.8	20.196	0.4394	0.3
11.108	0.7959	1.6	21.378	0.4153	0.4
11.261	0.7852	3.6	23.01	0.3862	1.4
12.299	0.7191	3.3	23.565	0.3772	1.2
12.56	0.7042	1.4			

Table 3.6 - X-ray powder diffraction pattern obtained for Cu-Stearate, most intense peaks in BOLD

2θ (°)	d-spacings (nm)	I/Io (%)	2θ (°)	d-spacings (nm)	I/I° (%)
6.194	**1.4257**	**100.0**	**19.823**	**0.4475**	**19.1**

8.265	1.0689	10.1	20.382	0.4354	3.1
10.388	**0.8509**	**37.0**	21.741	0.4085	3.8
10.87	0.8133	14.5	22.404	0.3965	3.9
11.532	0.7666	9.3	22.816	0.3895	3.1
12.438	0.7111	7.6	23.446	0.3791	5.1
14.525	0.6093	6.9	24.091	0.3691	3.0
18.752	0.4728	1.6	25.953	0.3430	0.8

Table 3.7 - X-ray powder diffraction pattern obtained for Cu-Oleate, most intense peaks in BOLD

The effect of carbon chain unsaturation on the diffraction patterns can be observed by comparing the patterns obtained for Cu-Stearate (Table 3.6) with those obtained for Cu-Oleate (Table 3.7). The highest intensity peak of Cu-Oleate has a d-spacing (1.4257nm) in the same order as that of Cu-Palmitate (1.4139nm), not which has a shorter carbon chain, as reported in the literature [2, 17].

The diffraction patterns obtained for the copper soaps conform to the general structural arrangement of a metal soap where metal atoms form a mono cationic layer sandwiched by the carboxylate carbon chains [18]. The effect of this arrangement is high intensity long d-spacings at low angles, as the x-ray strikes the length of the metal soap dimer molecule, with the short d-spacings at higher angles corresponding to the chain packing arrangement [18].

3.1.5 Analysis by Mass Spectrometry Techniques

3.1.5.1 Direct mass measurement by Flow Injection Analysis (FIA)

Only the mass of the carboxylate ions could be found, but at extremely low counts, varying according to the solvent (Table 3.8). The low abundance of carboxylate ions may be a consequence of the strength of the bond between copper and carboxylate ligand. The low ion count for the carboxylate ions obtained in acetonitrile was expected as this solvent can chelate Cu(II) ions resulting in copper(I)-acetonitrile complexes [19]. Interestingly, copper(I)-acetonitrile complexes were identified in the Cu-Stearate (main ion peak) and Cu-Oleate. Both samples also yielded the highest relative amount of carboxylate ions.

	ion m/z	Ion abundance in		
		Acetonitrile	Chloroform	Methanol
Cu-Palmitate	255.2327	*	***	**
Cu-Stearate	283.2636	**	**	***
Cu-Oleate	281.2119	**	***	*

Cu-Linoleate	279.2317	*	*	**

KEY: * trace ** low ***medium in logarithmic scale

Table 3.8 - Copper soaps' relative solubility in selected solvents

3.1.5.2 Quadrupole Time-of-Flight Gas Chromatography with Tandem Mass Spectrometry with a Thermal Sample Probe (QTOF-GC-MS/MS with TSP)

Despite the presence of minor impurities, the chromatograms of Cu-Palmitate (Fig 3.7a), Cu-Stearate (Fig 3.8a) and Cu-Oleate (Figure 3.9a) all contained a large chromatographic peak corresponding to the carboxylic acid both in Electron Ionization (EI) and Chemical Ionization (CI) modes. For Cu-Linoleate, the largest peak in its chromatograms (Figure 3.10a) corresponds to azelaic acid ($C_9H_{16}O_4$) due to the oxidative cleavage of linoleic acid [20-22].

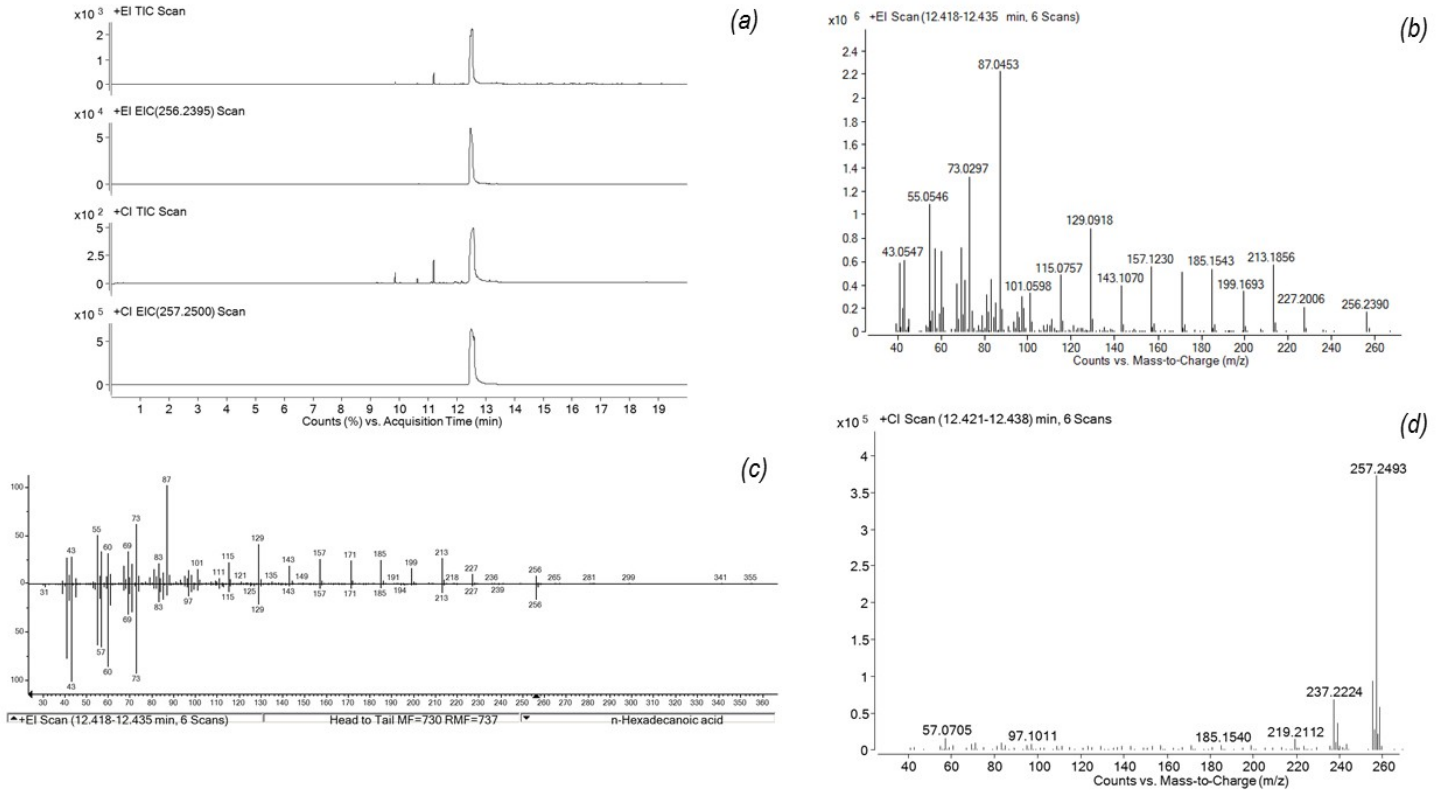

Fig 3.7 – Cu-Palmitate's EI and CI Chromatograms (a), Mass Spectra in EI (b) and CI (d), and NIST library match (c)

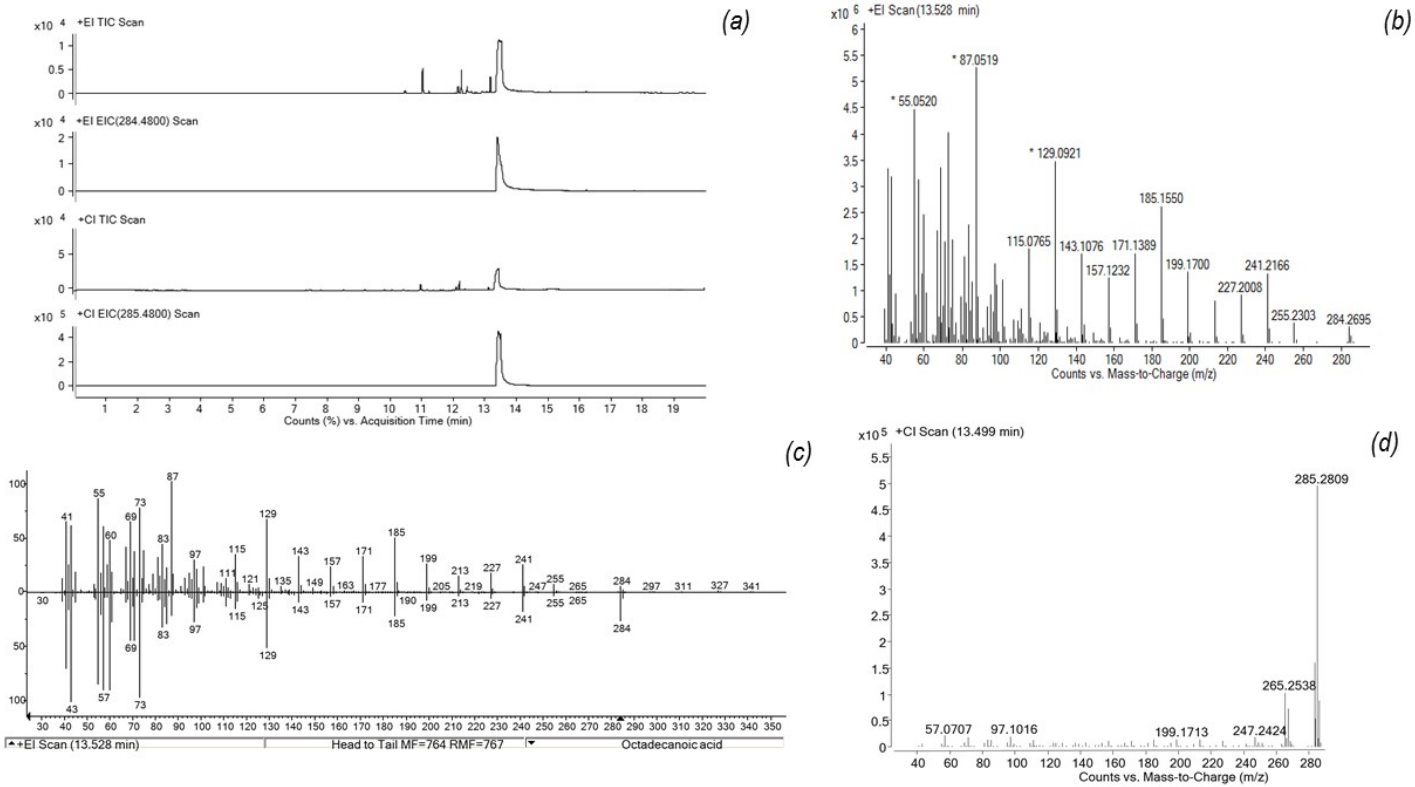

Fig 3.8 - Cu-Stearate's EI and CI Chromatograms (a), Mass Spectra in EI (b) and CI (d), and NIST library match (c)

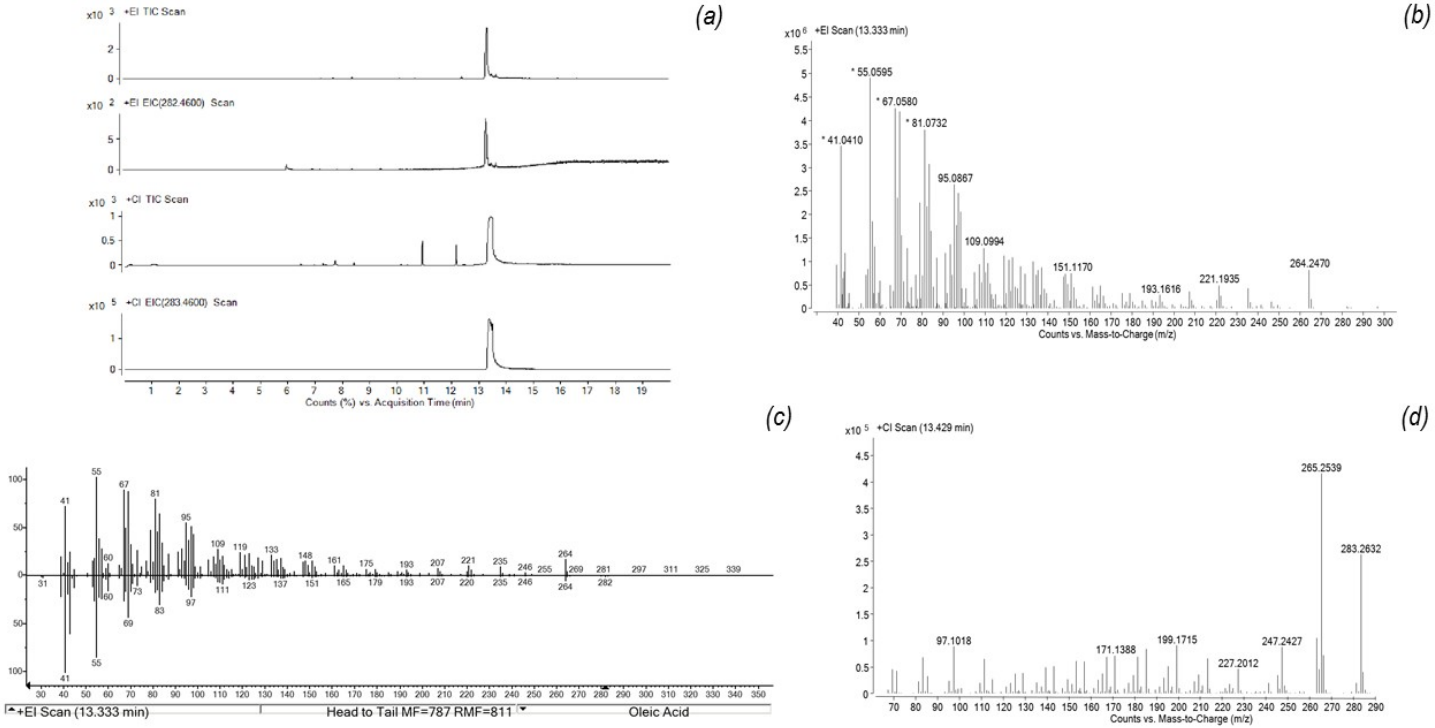

Fig 3.9 - Cu-Oleate's EI and CI Chromatograms (a), Mass Spectra in EI (b) and CI (d), and NIST library match (c)

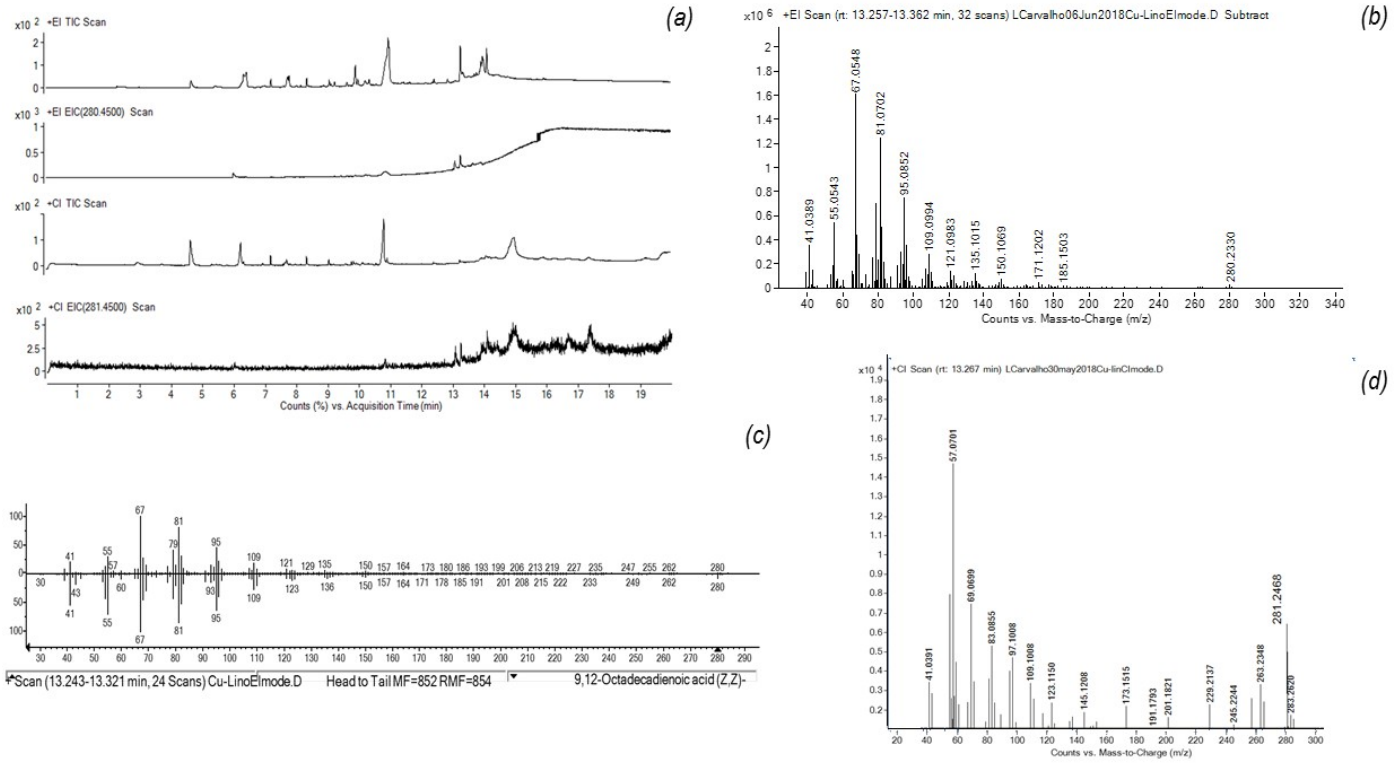

Fig 3.10 - Cu-Linoleate's EI and CI Chromatograms (a), Mass Spectra in EI (b) and CI (d), and NIST library match (c)

3.1.5.3 Solvent extraction with N, O-Bistrifluoroacetamide (BSTFA) derivatization followed by by Gas Chromatography with Mass Spectrometry (GC-MS)

Only the palmitic and stearic ligands (as methyl esters) were identified.

3.1.6 Discussion

The FTIR, Raman and XRD results largely agree with those published in the literature [11, 17]. Confirmation that copper is coordinating with oxygen ions was obtained by the strong peak at around 1580cm^{-1} in the FTIR spectra and the peaks under 450cm^{-1} in the Raman spectra.

The blue/green colour of the compounds indicated the presence of Cu(II) ions, which was confirmed by XPS. The XPS survey data also indicates that each Cu(II) ion coordinates with two carboxylate ions in a dimer arrangement, leading to the long d-spacings observed in the XRD data. This stoichiometry could not be confirmed for Cu-Linoleate, possibly because the sample was damaged/degraded before or during data acquisition [23].

The results obtained from the mass spectrometry analyses differed. Only the saturated ligands were identified using the solvent extraction protocol. The low solubility of metal soaps in organic solvents has long been recognized as a drawback to GC-MS protocols that include solvent extraction [24]. However, the results obtained indicate that the bond between copper ions and palmitate/stearate may have a more ionic character (making these soaps more soluble) than the bond with oleate/linoleate ligands.

3.2 Characterization of Cu-Lactose

The (+) coupon at the end of the experiment with the electrolyte containing lactose was covered by a blue powdery deposit (Fig 3.1e), from this point onwards referred to as Cu-Lactose.

3.2.1 Analysis by FTIR

Saccharides usually bind to a metal ligand via deprotonation of one or more hydroxyl groups [25-26]. Lactose is a disaccharide consisting of one galactose unit linked to a glucose unit by an O-glycosidic bond. Given its many hydroxyl groups, many modes of coordination with metal ions are possible.

The spectra of lactose and Cu-Lactose are very similar (Fig 3.11) with the most characteristic peak being the hydroxylated broad band centred around 3400cm^{-1} (Table 3.9). For lactose, this band contains small peaks at 3453, 3392 and 3294cm^{-1} due to its high level of crystallinity [27-28]. In Cu-Lactose (Fig 3.11b) these small peaks disappear due to the presence of water molecules [29] trapped within the complex during synthesis of the complex. The three sharp bands at 1480-1300cm^{-1}, 1160-890cm^{-1} and 660-460cm^{-1} shift to around 1400cm^{-1}, 1080cm^{-1} and 500cm^{-1} interaction [26, 29].

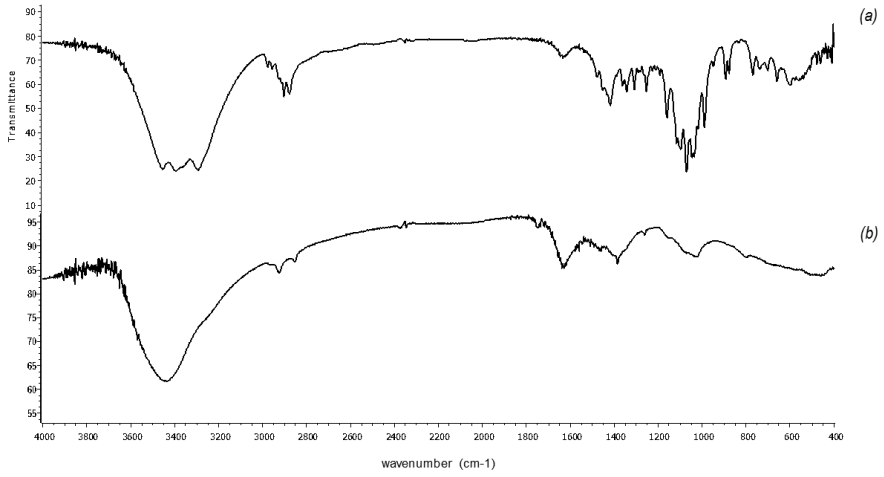

Fig 3.11 - FTIR spectra of Lactose (a) and Cu-Lactose (b) obtained by the KBr method

Lactose		Cu-Lactose		Band Assignments
3744-3000	br	3694-3003	br	OH stretching vibration
2978	w			CH stretching vibrations
2957	w			CH stretching vibrations
2903	m			CH symmetric vibration of CH_2OH group
2878	m	2853	w	CH asymmetric vibration of CH_2OH group
1454	w			H-CH group scissoring vibrations
1417	m			CH_2 wagging (galactose)
1361	m			OCH deformation
1343	m			CCH deformation
1253	m			C-H rocking, OH rocking (glc)
1160	s	1160-890	br	C-O-C stretching vibration (glc)
1097	m			C-O-C stretching vibrations (gal)
1070	s			C-C stretching vibrations (gal)
990	m			C-H out-of-phase ring stretching and twisting
892	m			C-H out-of-phase ring stretching and twisting
597	m			OCO in-plane bending (gal)
461	m			C-C-O in-plane bending (glc)

br (broad), vs (very strong), s (strong), m (medium), w (weak), gal (galactose) and glc (glucose)

Table 3.9 - Main FTIR peaks for Lactose and Cu-Lactose with band assignments

3.2.2 Analysis by Raman

The shape of the spectrum of Cu-Lactose indicates fluorescence from the complex itself or impurities within it (Fig 3.12b).

Fluorescence results from the emission of energy absorbed by the molecule as they return to a lower state of energy. If the laser excitation energy is close to the electronic transition energy of the molecule, fluorescence may obscure Raman scattering [30].

The most common method for overcoming fluorescence is to use a laser with lower wavelengths [30-31], but none were available. Attempts were made to reduce the fluorescence by photobleaching the sample and by analysing Cu-Lactose directly off the copper coupon (as opposed to removing it to a glass slide) – both without success.

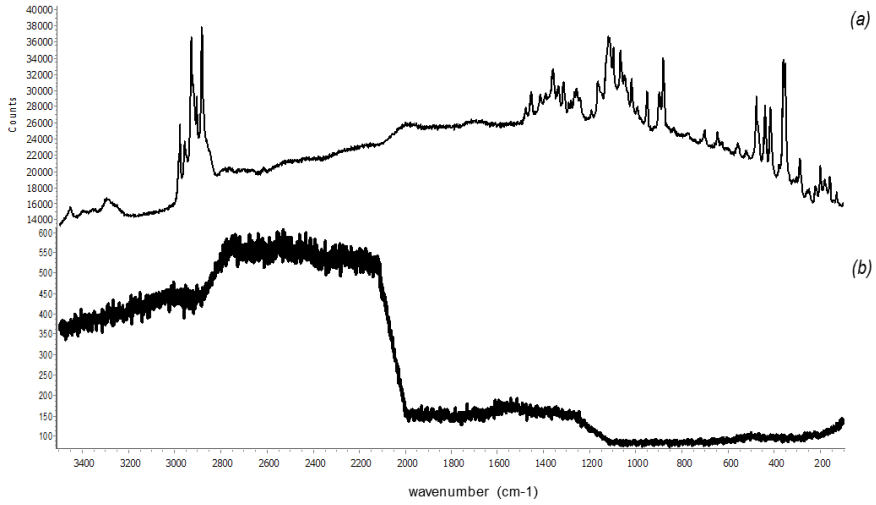

Fig 3.12 - Raman spectra of Lactose (a) and Cu-Lactose (b)

3.2.3 Analysis by XPS

The elemental composition measured for lactose as relative atomic percentages was 52.4% carbon, 43.5% oxygen and 4.1% silicon. Despite the silicon contamination, these values are close to those reported for anhydrous α/β lactose [32]. For Cu-Lactose, the relative atomic percentages were 43.3% carbon, 41.0% oxygen and 15.7% copper; its Cu2p spectrum contained the characteristic satellite peaks indicating the presence of Cu(II) ions.

The C1s and O1s spectra for lactose and Cu-Lactose also differed (Fig 3.13). In the copper complex, the peaks are broader due to charging of the sample during data collection, affecting particularly the carbon species. Consequently it is possible to decompose the C1s spectra of Cu-Lactose in more than three peaks (Figure 3.13c), with the extra peak centred at 285.84eV.

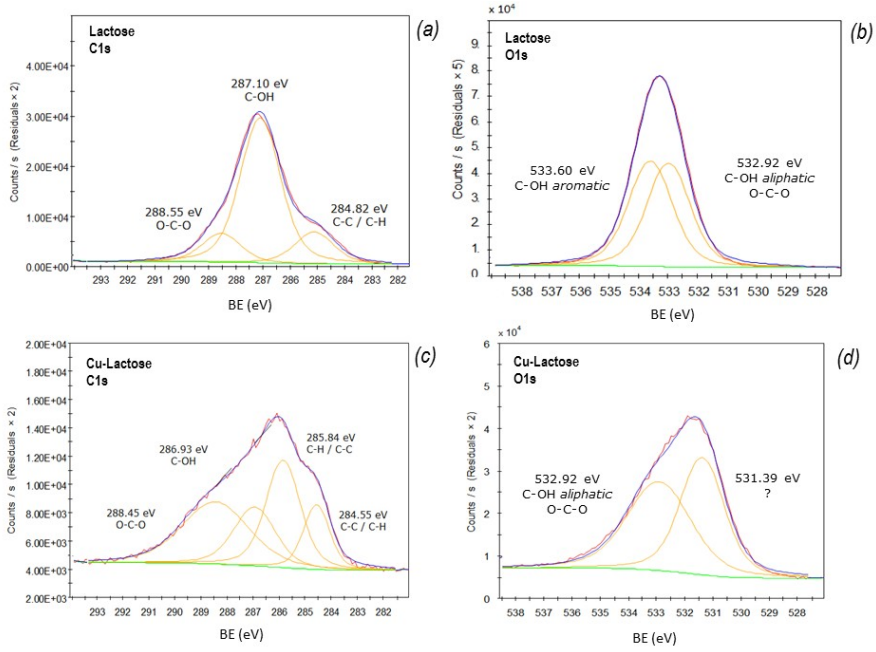

Fig 3.13 - Spectra of C1s and O1s regions of Lactose (a-b) and Cu-Lactose (c-d)

The O1s spectra for lactose and Cu-Lactose also differ. Complexation with copper resulted in the disappearance of the C-OH aromatic peak at 533.60eV and the appearance of a new peak centred at 531.39eV (Figure 3.13d). Although dehydroxylation of saccharides can occur during XPS analysis [32], there was no sign of degradation of the Cu-Lactose sample during or after analysis. Therefore, the peak at 531.39eV in the Cu-Lactose O1s spectra could be attributed to Cu-O bonds, which in inorganic compounds appear between 530.99-531.25eV [14].

3.2.4 Analysis by XRD

The diffractogram obtained for Cu-Lactose (not shown) was practically continuous. The few peaks present could be assigned to a cuprite (Cu_2O) phase in a largely amorphous sample.

3.2.5 Analysis by Mass Spectrometry Techniques

3.2.5.1 Direct mass measurement by FIA

No ion corresponding to Cu-Lactose was found in any of the solvents. Lactose, albeit at low ion counts, was identified in all solvents. Its with highest relative ion count was achieved in acetonitrile, where ions corresponding to copper-acetonitrile complex were also identified.

3.2.5.2 QTOF-GC-MS/MS with TSP

Lactose converts into its monosaccharide units after long exposure to temperatures above 180ºC [33], yielding characteristic anhydro sugars and furan derivatives at 650ºC [34]. The high number of chromatographic peaks – each representing at least one compound – obtained for Cu-Lactose in EI and CI modes (Figure 3.14) was therefore expected as the thermal separation probe (set at 320ºC) acts as a low temperature pyrolysis chamber. The identification of levoglucosenone (peak 4 in Figure 3.14) is therefore significant, as this compound is a derivative of levoglucosan and a pyrolysis product of glucose [35] and lactose [36].

The chromatograms for Cu-Lactose contain bigger peaks for fatty acids (4 and 5 in Fig 3.14) than those found in the lactose chromatograms (not shown). As the same amount of lactose and Cu-Lactose were analysed, this result may indicate copper's preference for forming complexes with carboxylic acids originally present in lactose as contaminants. A strong 61m/z peak, (Fig 3.14b) and peak 3 (identified as 5-acetoxynethyl-2-furaldehyde) were not observed in lactose's chromatograms. Their presence may be explained by catalytic effect of Cu(II) ions, which lowers the decomposition temperature of carbohydrates. For cellulose, this effect has translated into to higher yields of acetic acid, furans and gases [37].

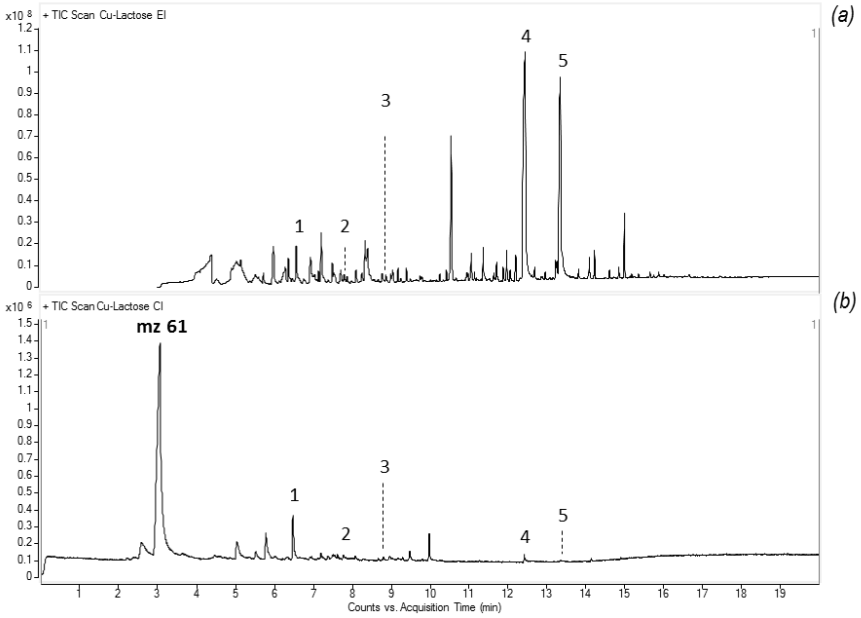

Fig 3.14 - EI (a) and CI (b) chromatograms for Cu-Lactose [1] 2H-Pyran-2,6(3H)-dione; [2] levoglucosenone; [3] 5-acetoxymethyl-2-furaldehyde; [4] n-hexadecanoic acid and [5] octadecanoic acid

3.2.6 Discussion

The characterization of Cu-Lactose by FTIR/Raman was complicated by poor peak definition and fluorescence. The XPS data confirmed the presence of Cu(II) ions within the compound suggesting coordination via the deprotonation of hydroxyl groups of the saccharide molecule. The identification of a cuprite phase by XRD is not surprising given that the glucose moiety in lactose is a reducing agent via its free aldehyde function that easily oxidises to acid [20].

The mass spectrometry characterization of the Cu-Lactose was only possible using the thermal separation probe method via identification of characteristic carbohydrate thermal decomposition products.

3.3 Characterization of Cu-Casein

The (+) copper coupon immersed in the electrolyte containing casein was covered by a translucent blue/greenish film at the end of the experiment (Figure 3.1f), which film peeled off upon drying out. From this point onwards this film will be referred to as Cu-Casein.

The structure of a protein is organized in four different levels. Its primary structure is determined by the amino acid composition of the main polypeptide chain and is dominated by covalent bonds between atoms. The folding of the polypeptide chain results in different types of interaction which are responsible for their secondary, tertiary and quaternary structures.

Bovine casein is a mixture of αs1-, αs2-, β-, κ-casein and other proteinaceous impurities. Despite having many hydrophobic amino acids, caseins have an open hydrated structure with areas of high negative charge enabling them to form colloidal aggregates [38].

Complexation between metal ions and proteins requires coordination with a donor atom, possibly via the deprotonation of a nitrogen from an amino group, the oxygen from a carboxylic acid group, and/or by interactions with the π-electrons from aromatic rings in the side chain of amino acids. In milk, αs- and β-caseins bind Ca^{2+} ions at phosphorylated serine residues [39] providing stability to micelle structures [40].

3.3.1 Analysis by FTIR

The spectra (not shown) for casein and Cu-Casein were practically identical. The only minor differences between the FTIR bands of casein and Cu-Casein (Table 3.10) are the sharpening of the 3700-3300cm^{-1} broad band, a decrease in the amide I band from 1651 to 1647cm^{-1} and an increase in the amide II band from 1536 to 1540cm^{-1}.

Casein		Cu-Casein		Band Assignments
3700-3300	br	3700-3300	br	N-H and O-H stretching vibrations
3072	sh	3071	sh	Overtone of amide II band
2961	m	2961	m	NH_3+ and CH stretching vibrations
2870	vw	2877	w	CH stretching vibrations
1651	vs	1647	vs	Amide I band α helix (80% C=O stretching or COO^- asymmetric stretching vibrations; 10% C-N stretching vibrations and 10% N-H vibrations)
1536	s	1540	s	Amide II band and C=O stretching or COO^- asymmetric stretching vibrations
1335	vw	1335	vw	C-H deformation vibrations
1238	m	1238	m	Amide III α helix
1073	m	1070	m	C-C stretching vibrations

br (broad), sh (shoulder), vs (very strong), s (strong), m (medium), w (weak)

Table 3.10 - Characteristic FTIR bands in Casein and Cu-Casein

3.3.2 Analysis by Raman

The Raman spectrum of casein is arched due to fluorescence (Fig 3.15a). Fluorescence in proteins result from the movement of electrons in conjugated systems such as those present in double bonds of aromatic rings. Changes to these systems, , lead to fluorescence suppression as observed for Cu-Casein (Fig 3.15b).

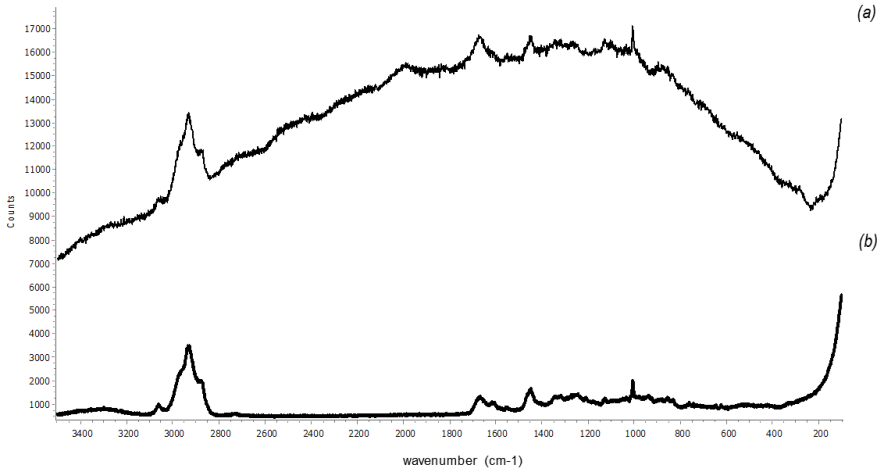

Fig 3.15 - Raman spectra of Casein (a) and Cu-Casein (b)

Despite the issues with fluorescence a few band assignments were still possible (Table 3.11).

Casein		Cu-Casein		Band Assignments
3061	w	3061	w	Overtone of amide II band
2934	vs	2934	m	Asymmetric CH_2 stretching
2879	sh	2879	sh	Symmetric CH_2 stretching
1673	s	1670	s	Amide I band (random chain) and COO^- asymmetric stretching vibration
1555	w	1555	w	Amide II band
1323	vw			Amide III band (incl. CN stretching, NH bending, C-O stretching, O=C-N bending etc)
1211	w	1211	w	C-O vibrations
1073	m	1070	m	C-C stretching vibrations

sh (shoulder), vs (very strong), s (strong), m (medium), w (weak), vw (very weak)

Table 3.11 - Characteristic Raman bands of Casein and Cu-Casein

The results obtained from FTIR and Raman are not surprising given how challenging metalloproteins are to analyse by these techniques, often requiring deconvolution and specific excitation to enhance the vibration of certain bonds. In the case of blue proteins – those that contain copper(II) ions - it is possible to observe shifts due to Cu-N, Cu-S or Cu-O bonds using a 600nm laser [3]. The Raman data was obtained with a 514nm laser.

3.3.3 Analysis by XPS

The relative atomic percentages obtained for casein were: 75.0% carbon, 16.96% oxygen and 8.03% nitrogen. Those for Cu-Casein were 72.2% carbon, 16.34% oxygen, 9.03% nitrogen, 0.6% phosphorus and 1.5% copper. The satellite peaks in the Cu2p spectrum of Cu-Casein indicates the presence of Cu(II) ions, assumed to be present given the characteristic blue colour of Cu-Casein.

The decomposed peaks for C1s and O1s and for N1s in casein and Cu-Casein are also informative (Fig 3.16). Peak decomposition and assignment are complicated by their broad shape due to sample charging and the structural complexity of casein, which contains a variety of chemical environments. Notwithstanding these difficulties, there are clear differences between the casein and Cu-Casein. The peaks of the C1s and O1s regions in Cu-Casein (Fig 3.16d-e) are narrower than casein's (Fig 3.16a-b), with the opposite effect observed for the N1s region (Fig 3.16c,f).

It is tempting to interpret an increased oxygen carboxylate peak at 531.69eV and, due to Brønsted donation [41], an increase in the nitrogen protonated amide peak at 401.61eV, as evidence of Cu(II) coordination with the second carboxylic acid groups of aspartic and glutamic acids in the peptide chain. These findings contrast with values observed in biological systems, where copper coordination is predominantly via nitrogen and sulfur donor atoms in the side chains of histidine, cysteine and methionine [42] and, at pH values above 10, with the amine of lysine [43]. The sensitivity of XPS compounded by the structural complexity of proteins means that such deductions would have to be confirmed by supplementary analysis such as magnetic nuclear resonance (NMR) or electron paramagnetic resonance (EPR) [44].

3.3.4 Analysis by XRD

The diffractogram obtained for Cu-Casein was similar to that obtained for Cu-Lactose. It was characteristic of an amorphous substance, with the exception of a peak above 35^{o} 2θ, identified as a Cu_2O phase.

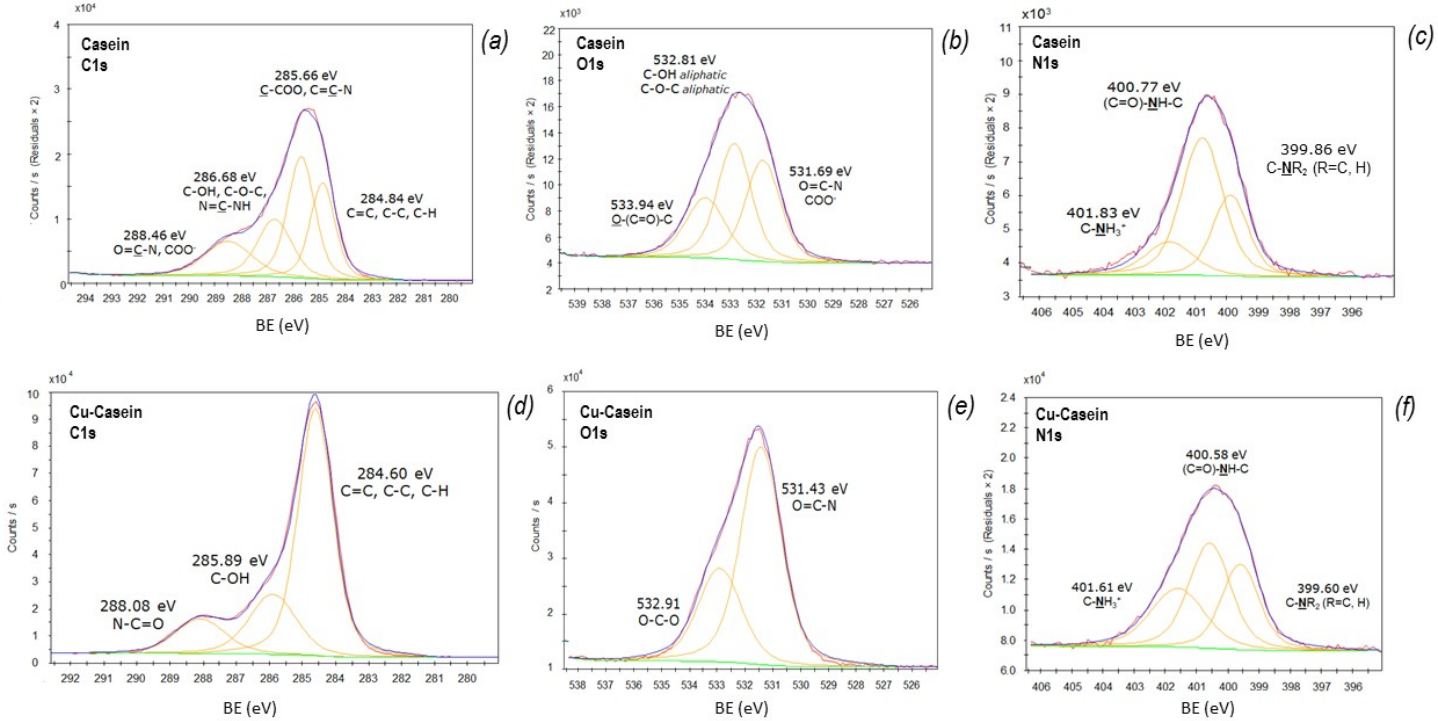

Table 3.16. Spectra of C1st, O1s and N1s regions of Casein (a-c) and Cu-Casein (d-f) peak fittings based on [45-46]

3.3.5 Analysis by Mass Spectrometry Techniques

3.3.5.1 Direct Mass Measurement by FIA

No high mass ions were detected in any of the solvents, indicating that Cu-Casein is not soluble in acetonitrile, chloroform or methanol.

3.3.5.2 QTOF-GC-MS

The peaks in the chromatograms for casein and Cu-Casein in EI mode (not shown) relate to nitrogen-containing aromatic compounds, products of the cyclisation of amino acids in the polypeptide chain subjected to pyrolysis [47].

Casein's chromatogram contained fewer peaks than Cu-Casein's. The extra peaks in the Cu-Casein chromatograms perhaps reflect specific thermal decomposition products associated with the presence of copper ions. Indole was the only compound identified in both EI and CI modes in Casein and Cu-Casein, one of the main products of the thermal degradation of bovine β-casein [48].

3.3.5.3 Proteomics

The four types of caseins were matched to the peptides recovered from casein and Cu-Casein (Table 3.12) albeit with different -10lgP values. The -10lgP value is a statistical indicator used to validate protein assignments (20 being the threshold for publication). Its values for the protein matches for casein and Cu-Casein are well above this minimal threshold, thus validating the extraction and digestion protocol used for these samples. The lower number of peptides identified in Cu-Casein may reflect metal complexation. Although metal chelation by proteins is extremely complex [49] and dependent on many factors [50], some tentative observations may be made by comparing the peptide coverage of casein and the Cu-Casein (Fig 3.17).

Protein	Average Mass (Da)	Coverage (%)		-10lgP*		# Peptides (# unique)	
		CSN	Cu-CSN	CSN	Cu-CSN	CSN	Cu-CSN
αs1-casein	24529	75	59	259.41	191.20	70 (68)	19 (19)
αs2-casein	26019	64	39	217.78	130.88	47 (47)	12 (12)
β-casein	25107	91	73	208.26	190.11	49 (49)	28 (28)
κ-casein	21269	71	43	247.12	194.55	64 (63)	18 (18)

* The -10lgP value is a statistical indicator used to validate protein assignments (20 being the threshold for publication).

Table 3.12. Protein matches for Casein (CSN) and Cu-Casein (Cu-CSN)

For αs1-casein (Fig 3.17a), half of the unidentified peptide residues in Cu-Casein contain tryptophan (W). Part of a group of amino acids that includes phenylalanine, tyrosine and histidine, tryptophan is reported to form non-covalent bonds with Cu(II) ions via the π-electrons from its aromatic ring [51-52]. The other half of the unidentified peptide fragments contain histidine (H), an essential metal chelating site [53]. Metal chelation with histidine is via its imidazole ring supported by the amino group [54] or a deprotonated amide nitrogen supported by a carboxylate oxygen [55].

For αs2-casein (Fig 3.17b), the unidentified peptide residues in Cu-Casein imply an interaction between histidine and glutamic acid (E) which could interact with Cu(II) ions via its deprotonated carboxylic groups. Metal complexation with the peptide chain of αs2-casein may also have been facilitated by its low hydrophobicity in relation to the other caseins.

For β-casein (Fig 3.17c), the unidentified peptide residues in the copper complex appear to indicate an interaction with glutamic acid alongside serine (S), with tryptophan and with proline (P). Proline is the only amino acid that contains a second amide, so Cu-N coordination is not possible [56]. Consequently, coordination with copper only happens when proline is in the N-terminal position of the peptide chain. In other positions, proline residues force the peptide chain to bend [57], thus facilitating the formation of macro-chelating sites [58].

An important caveat of the peptide coverage discussion is that the data is restricted to the most intense peptide fragments. Only further experiments and characterization with techniques such as NMR could elucidate metal-peptide chelation sites.

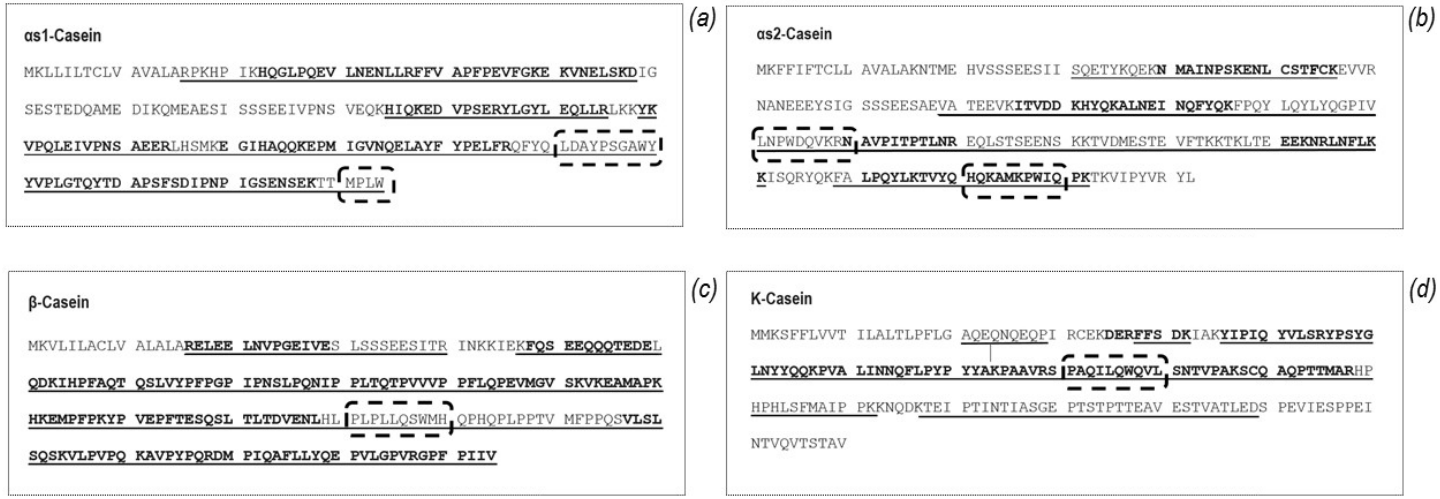

Fig 3.17 - Peptide chain for αs1-2-caseins (a-b) β-casein (c) and k-casein (d) with identified peptides in Casein (underlined) and Cu-Casein (in bold) with short peptide sequences containing tryptophan (W) within a dashed square. A list of amino acids abbreviations in included in the Appendix.

3.3.6 Discussion

Evidence of copper complexation with casein has been obtained with spectroscopic and mass spectrometry techniques. Notwithstanding the similarities between the FTIR spectra of casein and Cu-Casein, the slight changes on the bands of the latter indicate an interaction between copper and nitrogen/oxygen atoms. In Raman, the most obvious effect of copper complexation was the quenching of fluorescence, which may indicate coordination with amino acids containing aromatic rings.

Fluorescence in proteins usually arises from the amino acid residues phenylalanine, tyrosine and tryptophan (a popular marker for studying proteins' interaction with cofactors [59-64]).These amino acids are present in casein [65] and known to coordinate with Cu(II) ions [66-68].

The presence of Cu(II) ions in Cu-Casein, although anticipated by its blue colour, was confirmed by XPS. These ions appear to affect the thermal degradation of casein given that the chromatogram of the Cu-Casein obtained by GC-MS with TSP contained more peaks than that of pure casein. Nonetheless, indole, one of the main pyrolysis products of casein – was identified in casein and Cu-Casein.

The peptide fragments obtained from Cu-Casein matched all four types of caseins but at a lower coverage and intensity than those from pure casein. The difference in peptide coverage appears to correlate with sites of coordination when interpreted alongside the FTIR and Raman spectra. The data indicates different centres of interactions between the Cu(II) ions and deprotonated nitrogen, oxygen and amino acids containing aromatic rings as reported in the literature (for reviews on metal ion complexes see for example [69-70]) and as observed in blue copper proteins [42, 71-72].

References

[1] Socrates G (2001) Infrared and Raman Characteristic Group Frequencies. John Wiley & Sons, Chichester

[2] Satake I, Matuura R (1961) Studies with copper (II) soaps: Part I. Structural investigations of copper soaps and their complexes with pyridine and dioxane in solid state. Colloid Polym Sci 176(1):31-38

[3] Nakamoto K (1997) Infrared and Raman Spectra of Inorganic and Coordination Compounds. Part B: Applications in Coordination, Organometallics and Bioinorganic Chemistry. John Wiley & Sons Inc, New York/Chichester
[4] Gunn M, Chottard G, Rivière E, et al (2002) Chemical Reactions between Copper Pigments and Oleoresinous media. Stud Conserv 47(1):12-23
[5] Prati S, Bonacini I, Sciutto G, et al (2016) ATR-FTIR microscopy in mapping mode for the study of verdigris and its secondary products. Appl Phys A 122(1):1-16
[6] La Nasa J, Lluveras-Tenorio A, Modugno F, et al (2018) Two-step analytical procedure for the characterization and quantification of metal soaps and resinates in paint samples. Herit Sci 6(1):1-10
[7] Salvadó N, Buti S, Pradell T, et al (2019) Identification and Distribution of Metal Soaps and Oxalates in Oil and Tempera Paint Layers in Fifteenth-Century Altarpieces Using Synchrotron Radiation Techniques. In Casadio F, Keune K, Noble P, et al (eds) Metal Soaps in Art - Conservation and Research. Springer, Cham, p 195-210
[8] Mathey Y, Greig DR, Shriver DF (1982) Variable-temperature Raman and infrared spectra of the copper acetate dimer Cu2(O2CCH3)4(H2O)2 and its derivatives. Inorg Chem 21(9):3409-3413
[9] Conti C, Striova J, Aliatis I, et al (2014) The detection of copper resinate pigment in works of art: contribution from Raman spectroscopy: Detection of copper resinate pigment in works of art. J Raman Spectrosc 45(11-12):1186-1196
[10] Doyle A, Felcman J, Gambardella MTdP, Verani CN, et al (2000) Anhydrous copper(II) hexanoate from cuprous and cupric oxides. The crystal and molecular structure of Cu2(O2CC5H11)4. Polyhedron 19 (26-27):2621-2627
[11] Robinet L, Corbeil M-C (2003) The Characterization of Metal Soaps. Stud Conserv 48(1):23-40
[12] Frost DC, Ishitani A, McDowell CA (1972) X-ray photoelectron spectroscopy of copper compounds. Mol Phys 24(4):861-877
[13] Larson PE (1974) X-ray induced photoelectron and auger spectra of Cu, CuO, Cu2O, and Cu2S thin films. J Electron Spectros Relat Phenomena 4(3):213-218
[14] Biesinger MC, Lau LWM, Gerson AR, et al (2010) Resolving surface chemical states in XPS analysis of first row transition metals, oxides and hydroxides: Sc, Ti, V, Cu and Zn. Appl Surf Sci257(3):887-898
[15] Cano E, Torres CL, Bastidas JM (2001) An XPS study of copper corrosion originated by formic acid vapour at 40% and 80% relative humidity. Mater Corros 52(9):667-676
[16] Ávila-Torres Y, Huerta L, Barba-Behrens N (2013) XPS-Characterization of Heterometallic Coordination Compounds with Optically Active Ligands. J Chem 2013:1-9
[17] Corbeil M-C, Robinet L (2002) X-ray powder diffraction data for selected metal soaps. Powder Diffr 17(1): 52-60
[18] Corkery RW (1997) Langmuir–Blodgett (L–B) Multilayer Films. Langmuir 13(14):3591-3594
[19] Kolthoff IM, Coetzee JF (1957) Polarography in Acetonitrile. II. Metal Ions Which Have Significantly Different Polarographic Properties in Acetonitrile and in Water. Anodic Waves. Voltammetry at Rotated Platinum Electrode. JACS 79(8):1852–1858
[20] Morriosn RT, Boyd RN (1992) Organic Chemistry. Prentice-Hall International, London
[21] Asomaning J, Mussone P, Bressler DC (2014) Pyrolysis of polyunsaturated fatty acids. Fuel processing technology 120:89-95
[22] Sembiring KC, Minami E, Kawamoto H, et al (2020) Oxidative Cleavage of Linoleic and Linolenic Acids followed by Decarboxylation for Hydrocarbon Production. J Jpn Inst Energy 99:1-7

[23] Baer DR, Engelhard MH, Lea AS (2003) Introduction to Surface Science Spectra data on electron and x-ray damage: Sample degradation during XPS and AES measurements. Surf Sci Spectra 10(1):47-56
[24] La Nasa J, Modugno F, Aloisi M, et al (2018) Development of a GC/MS method for the qualitative and quantitative analysis of mixtures of free fatty acids and metal soaps in paint samples. Anal Chim Acta 1001:51-58
[25] Gottschaldt M,Wegner R, Görls H, et al (2004) Binuclear copper(II) complexes of 5-N-(β-ketoen)amino-5-deoxy-1,2- O-isopropylidene-α- d-glucofuranoses: synthesis, structure, and catecholoxidase activity. Carbohydr Res 339(11):1941-1952
[26] Cerchiaro G, Sant'Ana AC, Temperini MLA, et al (2005) Investigations of different carbohydrate anomers in copper(II) complexes with d-glucose, d-fructose, and d-galactose by Raman and EPR spectroscopy. Carbohydr Res340(15):2352-2359
[27] Norris KP, Greenstreet JES (1958) Infra-red Absorption Spectra of Casein and Lactose. Nature 181(4604):265-266
[28] Listiohadi Y, Hourigan JA, Sleigh RW, et al (2009) Thermal analysis of amorphous lactose and α-lactose monohydrate. Dairy Sci Technol 89(1):43-67
[29] Bandwar RP, Srinivasa Raghavan MS, Rao CP (1995) Transition metal-saccharide chemistry: d-glucose complexes of Mn(II), Co(II), Ni(II), Cu(II) and Zn(II). Biometals 8(1)
[30] Cebeci-Maltaş D, Alam MA, Wang P, et al (2017) Photobleaching profile of Raman peaks and fluorescence background. Eur Pharm Rev 22(6):18-21
[31] Kagan MR, McCreery RL (1994) Reduction of Fluorescence Interference in Raman Spectroscopy via Analyte Adsorption on Graphitic Carbon. Anal Chem 66(23):4159–4165
[32] Stevens JS, Luca AC, Pelendritis M, et al (2013) Quantitative analysis of complex amino acids and RGD peptides by X-ray photoelectron spectroscopy (XPS). Surf Interface Anal 45(8):1238-1246
[33] Paez M, Martinez-Castro I, Olano A (1987) Thermal degradation of different crystalline forms of lactose. J Anal Appl Pyrolysis 12(1):31-38
[34] da Silva PM, Gauche C, Gonzaga LV, et al (2016) Honey: Chemical composition, stability and authenticity. Food Chem 196:309-323.
[35] Pilath HM, Nimlos MR, Mittal A, et al (2010) Glucose reversion reaction kinetics. J Agric Food Chem 58(10):6131-6140
[36] Torri C, Lesci IG, Fabbri D (2009) Analytical study on the production of a hydroxylactone from catalytic pyrolysis of carbohydrates with nanopowder aluminium titanate. J Anal Appl Pyrolysis 84(1):25-30
[37] Terakado O, Amano A, Hirasawa M (2009) Explosive degradation of woody biomass under the presence of metal nitrates. J Anal Appl Pyrolysis 85(1):231-236.
[38] Alaimo MH, Farrell Jr HM, Germann MW (1999) Protein Structure and Molecular Enzymology. BBA 1431(2):410-420
[39] Dalgleish DG, Parker TG (1980) Binding of calcium ions to bovine αsl-casein and precipitability of the protein–calcium ion complexes. J Dairy Res 47(1): 113-12
[40] Dalgleish DG (2011) On the structural models of bovine casein micelles—review and possible improvements. Soft Matter (7):2265-227.
[41] Eggleston DS, Feldman SH (1990) Structure of the fibrinogen binding sequence: arginylglycylaspartic acid (RGD). Int J Pept Protein Res 36(2):161-166
[42] Rubino T, Franz KJ (2012) Coordination chemistry of copper proteins: How nature handles a toxic cargo for essential function. J Inorg Biochem 107(1):129-143
[43] Jeżowska-Bojczuk M, Stokowa-Sołtys K (2018) Peptides having antimicrobial activity and their complexes with transition metal ions. Eur J Med Chem 143:997-1009

[44] Stevenson MJ, Janisse SE, Tao L, et al (2020) Elucidation of a Copper Binding Site in Proinsulin C-peptide and Its Implications for Metal-Modulated Activity. Inorg Chem 59(13):9339-9349
[45] Rouxhet PG, Genet MJ (2011) XPS analysis of bio-organic systems. Surf Interface Anal 43(12):1453-1470
[46] Stevens JS, Luca AC, Pelendritis M, et al (2013) Quantitative analysis of complex amino acids and RGD peptides by X-ray photoelectron spectroscopy (XPS). Surf Interface Anal 45(8):1238-1246
[47] Moldoveanu Ș (1998) Analytical pyrolysis of natural organic polymers Elsevier, Amsterdam/New York
[48] Orsini S, Parlanti F, Bonaduce I (2017) Analytical pyrolysis of proteins in samples from artistic and archaeological objects. J Anal Appl Pyrolysis 124:643-657
[49] Kozlowski H, Potocki S, Remelli M, et al (2013) Specific metal ion binding sites in unstructured regions of proteins. Coord Chem Rev 257(19-20):2625-2638
[50] Dudev T, Lim C (2014) Competition among Metal Ions for Protein Binding Sites: Determinants of Metal Ion Selectivity in Proteins. Chem Rev 114(1):538-556.
[51] Remko, M., D. Fitz, R. Broer and B. M. Rode (2011) Effect of metal Ions (Ni2+, Cu2+ and Zn2+) and water coordination on the structure of L-phenylalanine, L-tyrosine, L-tryptophan and their zwitterionic forms. J Mol Model 17: 3117–3128
[52] Kadej A, Kuczer M, Czarniewska E, et al (2016) High stability and biological activity of the copper(II) complexes of alloferon 1 analogues containing tryptophan. J Inorg Biochem 163:147-161
[53] Rulíšek L, Vondrášek J (1998) Coordination geometries of selected transition metal ions (Co2+, Ni2+, Cu2+, Zn2+, Cd2+, and Hg2+) in metalloproteins. J Inorg Biochem 71(3-4):115-127
[54] Altun Y, Köseoĝlu F (2005) Stability of Copper(II), Nickel(II) and Zinc(II) Binary and Ternary Complexes of Histidine, Histamine and Glycine in Aqueous Solution. J Solution Chem 34:213-231
[55] Dunbar RC, Martens J, Berden G, et al (2018) Binding of Divalent Metal Ions with Deprotonated Peptides: Do GasPhase Anions Parallel the Condensed Phase? J Phys Chem A 122(25):5589-5596
[56] Siemion IZ, Kubik A, Jezowska-Bojczuk M, et al (1984) The absolute configuration on the chiral nitrogen atom of proline residue in the metal complexes of oligopeptides. J Inorg Biochem 22(2):137-141
[57] Krieger F, Möglich A, Kiefhaber T (2005) Effect of Proline and Glycine Residues on Dynamics and Barriers of Loop Formation in Polypeptide Chains. JACS 127(10):3346–3352
[58] Pettit LD, Steel I, Formicka-Kozlowska G, et al (1985) The L-proline residue as a 'break-point' in metal–peptide systems. Dalton Trans (3):535-539.
[59] Bent DV, Hayon E (1975) Excited state chemistry of aromatic amino acids and related peptides. III. Tryptophan. JACS 97(10):2612-2619
[60] Chen Y, Barkley MD (1998) Toward Understanding Tryptophan Fluorescence in Proteins. Biochem 37(28):9976–9982
[61] Vivian JT, Callis PR (2001) Mechanisms of Tryptophan Fluorescence Shifts in Proteins. Biophys J 80(5):2093-2109
[62] Tayeh N, Rungassamy T, Albani HR (2009) Fluorescence spectral resolution of tryptophan residues in bovine and human serum albumins. J Pharm Biomed Anal 50(2):107-116

[63] Li YH, Wang WJ, Xu XJ, et al (2015) Changes in fluorescence intensity induced by soybean soluble polysaccharide–milk protein interactions during acidification. J Dairy Sci 98(12):8577-8580

[64] Lai CW, Schwab M, Hill SC, et al (2016) Raman scattering and red fluorescence in the photochemical transformation of dry tryptophan particles. Opt Express 24(11):11654-11667

[65] Gordon WG, Semmett WF, Cable RS, et al (1949) Amino Acid Composition of α-Casein and β-Casein. J Am Chem Soc 71(10):3293–3297

[66] Davies RR, Kuang H, Qi D, et al (1999) Artificial metalloenzymes based on protein cavities: Exploring the effect of altering the metal ligand attachment position by site directed mutagenesis. Bioorg Med Chem Lett 9(1):79-84

[67] Reddy PR, Manjula P (2007) Mixed-ligand copper(II)-phenanthroline-dipeptide complexes: Synthesis, characterization, and DNA-cleavage properties. Chem Biodivers 4(3):468-480

[68] Husain A, Kumar G, Sood T, et al (2018) Synthesis, structural characterization and DFT analysis of an unusual tryptophan copper(II) complex bound via carboxylate monodentate coordination: Tetraaquabis(l-tryptophan) copper(II) picrate. Inorganica Chim Acta 482:324-332

[69] Bal W, Sokołowska M, Kurowska E, et al (2013) Binding of transition metal ions to albumin: Sites, affinities and rates. BBA 1830:5444-5455

[70] Sovago I, Varnagy K, Lihi N, et al (2016) Coordinating properties of peptides containing histidyl residues. Coord Chem Rev 327–328:43-54.

[71] Nakamura K, Go N (2005) Function and molecular evolution of multicopper blue proteins. CMLS 62(18): 2050-2066.

[72] Pérez-Henarejos SA, Alcaraz LA, Donaire A (2015) Blue Copper Proteins: A rigid machine for efficient electron transfer, a flexible device for metal uptake. Arch Biochem Biophys 584:134-148